

Article

Towards an Efficient Multi-Generation System Providing Power, Cooling, Heating, and Freshwater for Residential Buildings Operated with Solar-Driven ORC

Fahad Awjah Almehmadi ^{1,*} , Hassan Fawzy Elattar ^{2,3}, Ali Fouda ^{3,4}, Saeed Alqaed ⁵ , Mathkar A. Alharthi ⁶ 
and Hassanein Abdelmohsen Refaey ^{7,8,*} 

- ¹ Department of Applied Mechanical Engineering, College of Applied Engineering, Muzahimiyah Branch, King Saud University, P.O. Box 800, Riyadh 11421, Saudi Arabia
 - ² Department of Mechanical Engineering, Benha Faculty of Engineering, Benha University, Benha 13511, Egypt
 - ³ Department of Mechanical and Materials Engineering, Faculty of Engineering, University of Jeddah, Jeddah 21589, Saudi Arabia
 - ⁴ Department of Mechanical Power Engineering, Faculty of Engineering, Mansoura University, El-Mansoura 35516, Egypt
 - ⁵ Mechanical Engineering Department, College of Engineering, Najran University, P.O. Box 1988, Najran 61441, Saudi Arabia
 - ⁶ Department of Chemical Engineering, College of Engineering at Yanbu, Taibah University, Yanbu Al-Bahr 41911, Saudi Arabia
 - ⁷ Department of Mechanical Engineering, Faculty of Engineering at Shoubra, Benha University, Cairo 11629, Egypt
 - ⁸ Department of Mechanical Engineering, College of Engineering at Yanbu, Taibah University, Yanbu Al-Bahr 41911, Saudi Arabia
- * Correspondence: falmehmadi@ksu.edu.sa (F.A.A.); hassanein.refaey@feng.bu.edu.eg (H.A.R.)



Citation: Almehmadi, F.A.; Elattar, H.F.; Fouda, A.; Alqaed, S.; Alharthi, M.A.; Refaey, H.A. Towards an Efficient Multi-Generation System Providing Power, Cooling, Heating, and Freshwater for Residential Buildings Operated with Solar-Driven ORC. *Appl. Sci.* **2022**, *12*, 11157. <https://doi.org/10.3390/app12211157>

Academic Editor:
Luis Hernández-Callejo

Received: 1 October 2022
Accepted: 1 November 2022
Published: 3 November 2022

Publisher's Note: MDPI stays neutral with regard to jurisdictional claims in published maps and institutional affiliations.



Copyright: © 2022 by the authors. Licensee MDPI, Basel, Switzerland. This article is an open access article distributed under the terms and conditions of the Creative Commons Attribution (CC BY) license (<https://creativecommons.org/licenses/by/4.0/>).

Abstract: In buildings, multi-generation systems are a promising technology that can replace discrete traditional energy production methods. A multi-generation system makes it possible to efficiently produce electricity, cooling, heating, and freshwater simultaneously. This study involved the numerical analysis of a modified proposed novel solar-driven multi-generation system (MGS-II) integrated with the Organic Rankine Cycle (ORC), Humidification–Dehumidification Desalination System (HDH), and Desiccant Cooling System (DCS) by using heat recovery and thermal energy storage (TES) units. In addition, a comparison study with the basic multi-generation system (MGS-I) is performed. The proposed system is designed to supply electricity, air conditioning, domestic heating, and fresh water to small/medium-sized buildings. How operating conditions affect system productivity and performance metrics have been investigated. The results show that the proposed multi-generation system (MGS-II) can produce electrical power, space cooling, domestic heating and fresh water while maintaining comfortable conditions inside the conditioned space. Moreover, the MGS-II outperforms the MGS-I system, and the maximum MGS-II system productivity; electricity production (W_{net}^{\bullet}), freshwater (m_{fresh}^{\bullet}), space cooling ($Q_{cooling}^{\bullet}$), and domestic heating ($Q_{heating}^{\bullet}$) are 102.3 kW, 141.5 kg/h, 20.77 kW, and 225 kW, respectively. In addition, the highest total gained output ratio (TGOR), specific total gained energy (STG), and specific total gained energy equivalent price (STGP) of the MGS-II system are 0.6303, 3.824 kWh/m², and 0.149 USD/m², respectively. The accepted ranges of comfortable space-supplied air conditions (temperature and humidity) are 15.5–18.2 °C and 9.2–12.00 gv/kga for both systems, MGS-I and MGS-II. Finally, the current system (MGS-II) has the maximum of the system's performance indicators and productivity (TGOR and m_{fresh}^{\bullet}) compared with the other reported systems.

Keywords: multi-generation; humidification–dehumidification; desiccant cooling; Organic Rankine Cycle; heat recovery

1. Introduction

Multi-generation technology powered by renewable energy has piqued interest as a potential alternative to traditional energy production technology. It is applicable in a wide range of applications, particularly for small and medium-scale systems in buildings. It also provides a variety of technological, economic, energy recovery, and environmental advantages. The necessity for sufficient energy, fresh water, and cooling for human activities has been highlighted as a result of increased industrial growth and population [1]. Renewable energy sources are seen as a long-term answer to meeting energy, fresh water, and cooling/heating production needs, especially in buildings. The availability of energy supplies and global warming are two key problems for the future sustainability of energy production. As a result, converting to renewable resources and developing more energy-efficient and ecologically friendly technologies is more important than ever. Renewable energy-based hybrid systems can reduce the use of fossil fuels and CO₂ emissions, while also being suitable for regional applications [2]. Solar energy has emerged to be one of the most popular renewable energy sources since it is non-polluting and has an endless supply.

Recently, it has been suggested to use tri/multi-generation systems in buildings. Tri-generation systems, which include cooling, heating, freshwater production, and power generation, are considered an efficient approach for reducing primary energy use and greenhouse gas emissions in buildings. Through an energetic, economic, and environmental performance assessment, Wang et al. [3] demonstrated that a tri-generation system's combined cooling and heating mode is considerably better than an independent HVAC system. Ahmadi et al. [4] have presented a new residential multi-generation system. Heating, cooling, power generation, hydrogen creation, and hot water production are all part of the system. When compared to a single-generation system, multi-generation from waste heat can increase the system's energy efficiency by around 60% and nearly double its exergy efficiency. Liu et al. [5] presented a hybrid energy supply system combining GEHPs (engine-driven heat pumps) and ORCs to provide heating, cooling, hot water, and electricity for buildings. Working fluids used in the ORC system are R245fa, R152a, and R123. According to the findings, waste heat recovered from gas engines accounts for more than 55% of gas engine energy consumption. R123 also has the highest thermal and exergy efficiency in the ORC system, with 11.84% and 54.24%, respectively.

The current tri/multi-generation technologies can offer a variety of benefits [6], including lower carbon dioxide equivalent emissions, increased global energy efficiency while expanding renewable energy sources, and decreased electrical system overloads and blackouts. Only a few researchers have focused on modelling tri/multi-generation systems that combine renewable energy resources with electricity, cooling or heating, and freshwater generation. Zhang et al. [7] investigated a hybrid solar-biomass tri-generation system for producing hot water, power, and chilled water. Their simulation and performance analysis of the tri-generation system was carried out to evaluate the influence of key operating parameters on the system's performance. Maraver et al. [8] investigated the use of a biomass system to power a poly-generation cycle that produces electricity, fresh water, cooling, and heat. A small-scale ORC engine, a MED (multi-effect desalination) plant, and an LBSE (lithium bromide–water simple effect) absorption chiller is all part of their proposed poly-generation system. They concluded that the quantity of heat produced in the ORC condenser, which is used for desalination, drastically limits the primary energy savings compared to typical systems, as well as the electric efficiency obtained with each individual fluid. In addition to, Gholizadeh et al. [9] designed a new biogas-powered tri-generation system for power generation, cooling, and drinking water. An ORC and an ejector cooling cycle (ECC) are included in the system, as well as an HDH and a gas turbine (GT). The system's optimization increases net power, cooling, TGOR, and exergy efficiency by 2.58%, 22.69%, 14.04%, and 13.26%, respectively. Regarding multi-objective optimization factors, Baghernejad et al. [10] investigated three tri-generation energy systems (biomass tri-generation, solid oxide fuel cell tri-generation, and integrated solar tri-generation). The

solid oxide fuel cell tri-generation system is determined to have the greatest tri-generation exergy efficiency at 64.5%.

Zare [11] provided a thermodynamic analysis and optimization comparison of two separate designs of geothermal energy-based tri-generation systems based on research involving geothermal energy (one using an ORC and the other using a Kalina cycle). The ORC and Kalina cycles are coupled to a LiBr/water absorption chiller and a water heater to provide cooling and heating loads, respectively. In addition, Azhar et al. [12] investigated a multigenerational system that utilizes geothermal, solar, and ocean thermal energy conversion as energy inputs to produce electrical power, fresh water, space cooling, and industrial heating. The energy and exergy efficiency of the entire system were determined to be 13.93% and 17.97%, respectively. Moreover, Gholizadeh et al. [13] developed a unique tri-generation system that generates potable water, electricity, and cooling utilizing a flash-binary geothermal heat source at 170 °C. It was discovered that optimization increases turbine output power, overall cooling load, tri-generation-based gain-output-ratio (TGOR), and exergy efficiency by approximately 77.08 percent, 87.01 percent, 8.18 percent, and 46.33 percent, respectively. In addition, Li et al. [14] described a novel geothermal-powered tri-generation layout based on a cascade power system and a CO₂ cooling system. A modified Kalina cycle (MKC), an (ORC), and a liquefied natural gas (LNG) subsystem are all components of the geothermal-powered cascade system. The net output power, cooling rate, and hydrogen rate of the system are 451.8 kW, 297.8 kW, and 2.27 kg per hour, respectively.

In another studies, Hands et al. [15] tested a tri-generation power plant with solar desiccant air conditioning. The solar-driven desiccant cooling system met roughly 35% of the total building cooling load under ideal ambient circumstances. Abdelhay et al. [16] conducted a thermodynamic analysis of a poly-generation system that included a solar power system (SPS), a multi-effect desalination (MED) system, and an absorption refrigeration system (ARS). The facility is powered by solar energy, with a natural gas heater for backup. The proposed integrated system has the lowest unit water price of 1247 USD/m³, cooling unit price of 0.003 USD/kWhr, and the maximum energy efficiency of 23.95%. Dabwan et al. [17] devised and implemented a conceptual analytic approach for finding the optimal integration of linear Fresnel reflector (LFR) technology with traditional cooling, fresh water, and electric power tri-generation systems. Yao et al. [18] designed and evaluated a new tri-generation plant for integrated cooling, heating, and power based on compressed air energy storage technology. It was discovered that choosing the best trade-off solution resulted in an overall exergy efficiency of 53.04% and a total product unit cost of 20.54 cents/kWh. Bellos and Tzivanidis [19] used several optimization parameters to optimize a tri-generation system for solar-powered building applications. According to the final results, the optimum system has an exergy efficiency of 11.26% and an energy efficiency of 87.39%, while the power outputs for electricity, cooling, and heating are 4.6 kW, 7.1 kW, and 59.4 kW, respectively. Recently, Fouda et al. [20] evaluated a unique tri-generation system for simultaneously generating electrical power, air conditioning, and desalinated water. The proposed system includes an ORC, a Humidification and Dehumidification (HDH) water desalination system, a Desiccant Cooling System (DCS), a solar system (including evacuated tube collectors and a thermal energy storage unit), and additional components. The proposed trigeneration system has the greatest electrical power, freshwater capacity, space cooling capacity, and Energy Utilization Factor (EUF) of 104.5kW, 72.37kg/h, 25.48kW, and 0.266%, respectively.

According to the literature review, few tri/multi-generation systems for power, fresh water, and cooling load combined with MED/SRC/ARS, HDH/ORC/ECC, and HDH/ORC/DCS operated with solar, biomass, biogas, and geothermal energies. As a result, multi-generation systems have not been thoroughly investigated to date. Therefore, a new multi-generation set-up based on an ORC, DCS, and HDH unit to generate power, space cooling/domestic heating, and fresh water is aimed to small/medium-scale buildings. The low operating temperatures are suitable for ORC power generation [21]. HDH water

desalination has several advantages, including low-temperature energy utilization (e.g., waste energy, solar energy), simplicity, and inexpensive operation and installation costs [22]. Desiccant air conditioners do not produce polluting gases such as chlorofluorocarbons, which are produced by traditional air conditioning systems. Therefore, these constraints motivate the authors to research the design, operation, and performance assessment of multi-generation systems capable of providing continuous daylight electrical power, fresh water, and space cooling/domestic heating using solar energy for small and medium-scale buildings.

To the authors' knowledge, no previous research into such advanced systems has been done. Therefore, a more efficient multi-generation system, including ORC, HDH, DCS, and with heat recovery systems is proposed, thermodynamically evaluated and compared with the basic system [20] in this study. The impact on the system's productivity and performance parameters is investigated using thermodynamics analysis and parametric study. The systems' cycles are thermodynamically simulated and analyzed using the EES (Engineering Equation Solver) software. The following points will be fulfilled: (i) extensive energy mathematical modeling, (ii) effects of various operating parameters on the system's productivity and performance, and (iii) assessing and evaluating the proposed system compared with basic system. It is expected that the findings of the proposed integrated ORC, HDH, and DCS multi-generation systems will attract attention and benefit researchers, solar multi-generation developers, power plant designers, and investors because of their economic and environmental feasibility for producing electricity, space cooling, domestic heating, and fresh water for end users, especially for small and medium-scale buildings.

2. Systems Description

Figure 1 depicts a schematic design of the basic system, and the modified suggested solar-driven multi-generation system with a heat recovery unit (MGS-I and MGS-II). By connecting solar ORC to a DCS and HDH desalination unit, the suggested system is designed to produce power, space cooling/domestic heating, and fresh water. An evacuated tube solar collector and a thermal storage tank are components of the solar system. A thermal oil (Therminol-VP1) is utilized as the working fluid for the solar field loop because of its capacity to maintain the liquid phase at temperatures up to 400 °C [23]. The basic system (MGS-I), which serves as a reference system, and the modified system are the systems that were investigated (MGS-II). As depicted in Figure 1, the MGS-I can produce energy, space cooling, and freshwater (a). The system has four major cycles: two closed cycles (the solar and the ORC) and two open cycles (air and water cycles).

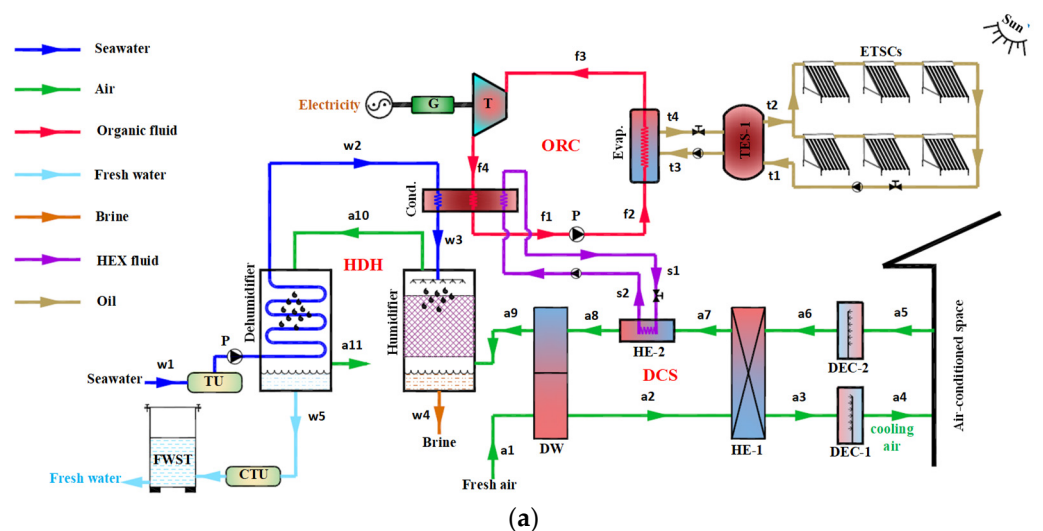


Figure 1. Cont.

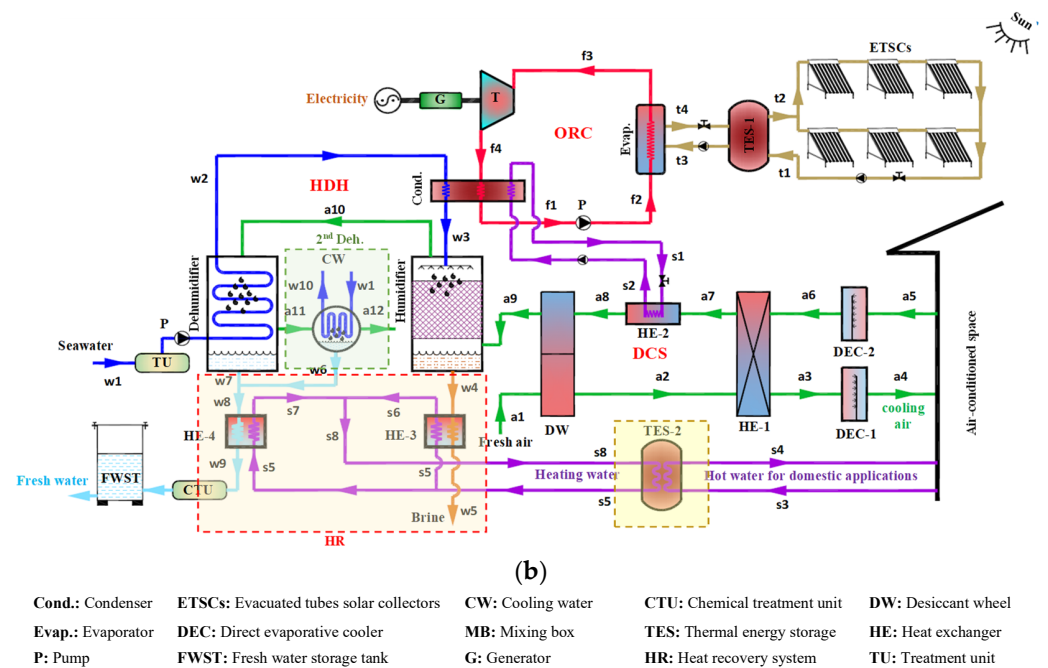


Figure 1. Schematic diagram of proposed multi-generation systems: (a) MGS-I; (b) MGS-II.

In the solar field cycle, evacuated tube solar collectors are used to charge the TES-1 tank when it is sunny (state points t1 and t2), which is then used to provide the system with constant energy demand through the ORC evaporator both during the day and at night (state points t3 and t4). The ORC cycle uses an evaporator to transfer heat from the thermal oil to the ORC fluid, which is then expanded through the turbine to produce electricity using a linked generator after becoming superheated to (f3) and evaporating. To maintain the same temperature at the state points (a8 and w3), the ORC fluid exits the turbine at (f4). It is delivered to the triple channel heat exchanger’s condenser, where it is condensed at (f1), and waste heat is recovered for the DCS and HDH units. The cycle is finished by pumping the ORC liquid to (f2) and then back to the evaporator. The ORC fluid leaves the turbine at position (f4). It is transported to the triple channel heat exchanger’s condenser, where it condenses at position (f1) and recovers waste heat for the DCS and HDH units to maintain the temperature at state points (a8 and w3). To complete the cycle, the ORC liquid is subsequently piped to (f2) and finally pushed back to the evaporator.

Process air enters the desiccant wheel (DW) at (a1) in the air cycle, where it is dehumidified and heated to (a2) before passing via the heat exchanger (HE-1), where it is cooled to (a3). The process air enters the direct evaporative cooler (DEC-1), which is cooled and humidified at (a4) before entering the air-conditioned chamber. The return air from the conditioned space at (a5) is directed to the direct evaporative cooler (DEC-2), where it is cooled and humidified before leaving at (a6). The heat exchanger (HE-1) is then used to heat the return air (a7). The return air (regeneration air) then passes through a heat exchanger (HE-2) to recover some of the waste ORC condenser heat to reach the necessary regeneration temperature (a8) before passing through DW (reactivation part), where it is cooled and humidified to the required regeneration temperature (a9). Finally, the HDH system delivers the humidified and cooled regeneration air from the DW to the humidifier, where it is humidified and cooled at (a10) before being given to the dehumidifier and is dehumidified at (a11). Figure 2a for the basic multi-generation system shows the psychrometric cycle of the air (MGS-I).

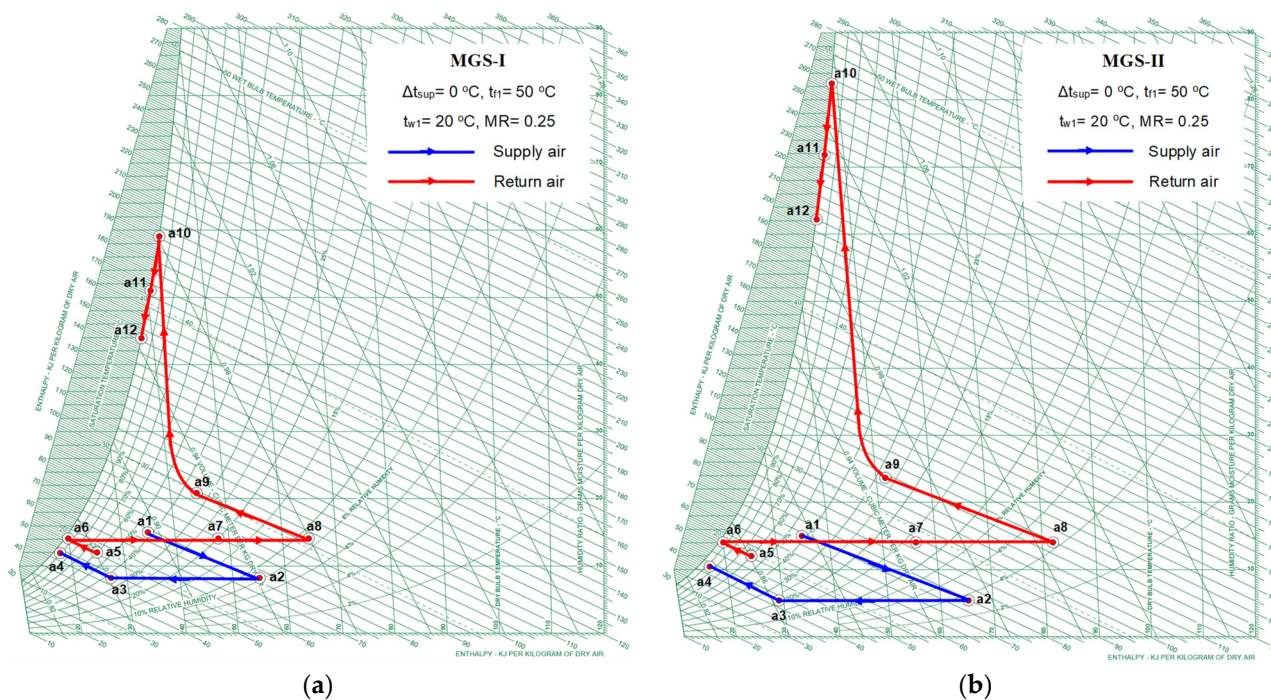


Figure 2. Psychrometric cycles of proposed multi-generation: (a) MGS-I; (b) MGS-II.

In the water cycle, seawater at (w1) is pumped through the water treatment unit (TU) to remove turbidity, bacterial content, and total dissolved solids, which cause fouling and scaling in the tubes and then passes through the dehumidifier coil to dehumidify the humid air that came from the humidifier to produce desalinated water at (w5). The desalinated water is sent through a chemical treatment unit (CTU) to make it fresh/potable water with a salinity of 500 ppm, which is the WHO's (World Health Organization) approved value. It is then gathered and stored in the FWST. The saltwater is heated to (w2) when it leaves the dehumidifier, and it then flows via an ORC condenser, where it is partially warmed using waste heat from the ORC condenser to reach (w3) before passing through a humidifier to moisten the air coming from the DW of DCS. The incoming air carries some of the pure water out to the dehumidifier as it evaporates, and the remaining pure water is drained as a brine at the end of the process (w4).

The schematic of the modified system (MGS-II) is shown in Figure 1b. The system can generate electricity, space cooling/domestic heating, and fresh water. The system consists of the same components and operations as the MGS-I. In addition, the system is improved by adding second stage dehumidification (2nd Deh.), a heat recovery system (HR), and a thermal energy storage unit to recover (TES-2) heat from brine and desalinated water to use in domestic heating applications. In MGS-II, the air leaves the first stage dehumidifier at (a11) and enters the second stage dehumidifier to reach (a12). The desalinated water yields at (w6) mix with the desalinated water produced from the first stage dehumidification (w7) to give the total desalinated water yields at (w8). After that, a heat recovery system is used to recover the heat energy from desalinated water (w8) and brine water (w4) to obtain heating water used for domestic applications via TES-2 to recover most of the waste heat. This helps to achieve system optimization and more efficient operation. The psychrometric cycle describing the processes of air through MGS-II is shown in Figure 2b.

3. Mathematical Model and Thermodynamics Analysis

The utilization of solar energy for the desalination of water, air conditioning, electricity generation, and hot water generation is being investigated and deployed in multi-generation systems intended for domestic applications. The multi-generation system is split into three subsystems, ORC, HDH, and DCS, to determine each subsystem's thermo-

dynamic characteristics and the entire system's performance. During the simulation model phase, the first and second laws of thermodynamics are applied to each system component. In the current model, the following assumptions have been considered:

- All system processes are assumed to be in a steady state.
- Air/water leakage in system components is ignored.
- The kinetic and gravitational energies are not considered.
- The air wet-bulb temperature and the blowdown water temperature leaving the humidifier are the same.
- Process air, return air, and water has the same mass flow rate.
- The cold outlet streams from ORC condenser are assumed to be the same ($t_{s1} = t_{w3}$) to distribute the condenser capacity on HDH and DCS cycles.
- At the dehumidifier's exit, the fresh water and the air wet-bulb temperatures are the same.
- The ORC fluid's states at the turbine inlet are dry-saturated and superheated based on the different values of t_{evap} and degree of superheating.
- Based on the pressure of the condenser, the ORC fluid state at the pump inlet is saturated liquid.
- In DCS and HDH systems, the special power of auxiliary components (power consumed by fans) is ignored.
- Organic fluid (n-Octane) is selected to carry out the comparative study of the proposed systems due to its performance and thermodynamic properties [24].
- The studied and operating parameters values, ranges, and relevant efficiencies for the system's components are given in Tables 1 and 2.
- Superheat degree at ORC turbine inlet and ORC evaporation temperature were selected based on the maximum temperature (200 °C) that can be obtained from the evacuated tube solar collectors and critical temperature of organic working fluids.
- ORC condensation temperature was selected based on the temperature of refrigerant in the condenser that should be greater than the heated air (t_{a7}) and sea water (t_{w2}) condensation temperature where the heat transfer process occurs in the right direction
- Mass flow rate ratio (0–0.4) was selected based on previously published work for HDH systems
- Ambient air inlet temperature, ambient air inlet humidity, seawater inlet temperature and average solar intensity were selected based on average climatic conditions of the Jeddah city, Saudi Arabia
- Conditioned space air temperature, and humidity were selected based on average inside design human comfort conditions.

Table 1. Studied and operating parameters; values and ranges.

Parameter	Value / Range
Superheat degree at turbine inlet, Δt_{sup}	0–45 °C
ORC evaporation temperature, t_{evap}	150 °C
ORC condensation temperature, t_{f1}	40–60 °C
ORC fluid mass flow rate, m_{ORC}	1 kg/s
Mass flow rate ratio, MR	0.1–0.4
Ambient air inlet temperature, t_{a1}	35 °C
Ambient air inlet humidity, w_{a1}	15 g _v /kg _a
Seawater inlet temperature, t_{w1}	15–25 °C
Conditioned space air temperature, t_{a5}	25 °C
Conditioned space air humidity, w_{a5}	12 g _v /kg _a
Average solar intensity, I_{avg}	0.8 kW/m ² (Jeddah city)

Table 2. Efficiencies of the systems components.

Parameter	Value
Dehumidifier efficiency, η_{Dh} [8].	0.95
Efficiency of the desiccant wheel, η_{F1} [25,26]	0.05
Efficiency of the desiccant wheel, η_{F2} [25,26]	0.95
Efficiency of evaporative cooler-1, η_{DEC-1} [25,26]	0.9
Efficiency of evaporative cooler-2, η_{DEC-2} [25,26]	0.9
Efficiency of heat exchangers, $\eta_{HE-1}, \eta_{HE-2}, \eta_{HE-3}, \eta_{HE-4}$ [25,26]	0.8
Efficiency of heat exchanger, η_{HE-2} [25,26]	1.0
Efficiency of the evacuated tube solar collector, η_{solar} [27]	0.632
Efficiency of electrical generator of ORC, η_g [28]	0.95
ORC pump efficiency, η_{pump} [28]	0.85
ORC turbine efficiency, $\eta_{turbine}$ [28]	0.85

As productivity metrics for the multi-generational systems are under study, electrical power generation (\dot{W}_{net}), freshwater productivity (\dot{m}_{fresh}), space cooling capacity ($\dot{Q}_{cooling}$), and home heating capacity ($\dot{Q}_{heating}$) are employed. The system’s performance is measured by the total gained output ratio (TGOR), specific total gained energy (STG), specific total gained energy equivalent cost (STGP), gain output ratio (GOR_{HDH}), coefficient of performance of DCS (COP_{DCS}), space supply air temperature and humidity ratio (t_4 and w_4), and area of solar collectors (A_{solar}). In the present multi-generational system, electrical power, space cooling capacity, freshwater productivity, and hot water production are all produced simultaneously from a single solar energy source.

3.1. Organic Rankine Cycle (ORC)

The organic working fluid (n-Octane), which has a low boiling temperature and an appropriate operating pressure within the parameter range of the solar energy heat source in the ORC system, is evaporated using solar energy. The governing equations (Equations (1)–(11)) of the evaporator, condenser, turbine, pump, and ORC thermal efficiency are presented in the following manner based on the energy and mass balance [20]:

- Evaporator energy balance

$$\dot{Q}_{Evap} = \dot{m}_{ORC} (h_{f3} - h_{f2}) \tag{1}$$

$$\dot{m}_{ORC} (h_{f3} - h_{f2}) = \dot{m}_{oil} (h_{t3} - h_{t4}) \tag{2}$$

$$\eta_{solar} = \frac{\dot{Q}_{Evap}}{\bar{I}_{T,avg,daily} A_{solar}} \tag{3}$$

The current work takes the total daily average solar intensity [8]. Whereas the average annual value of the thermal efficiency of the evacuated tube solar collector is 63.2%, [27]

- Condenser energy balance

$$\dot{Q}_{Cond} = \dot{m}_{ORC} (h_{f4} - h_{f1}) \tag{4}$$

$$\epsilon_{cond} = \left(\frac{\dot{m}_w (h_{w3} - h_{w2}) + \dot{m}_{R,a} (h_{a8} - h_{a7})}{\dot{m}_{ORC} (h_{f4} - h_{f1})} \right) \tag{5}$$

$$MR = \frac{\dot{m}_{ORC}}{\dot{m}_{R,a} + \dot{m}_w} \tag{6}$$

- Turbine power

$$W_t^\bullet = m_{ORC}^\bullet (h_{f3} - h_{f4}) \eta_t \eta_g \tag{7}$$

- Pump power

$$W_p^\bullet = m_{ORC}^\bullet v_{f1} (P_{f2} - P_{f1}) / \eta_p \tag{8}$$

$$W_p^\bullet = m_{ORC}^\bullet (h_{f2,a} - h_{f1}) \tag{9}$$

- ORC net power and thermal efficacy

$$W_{net}^\bullet = W_t^\bullet - W_p^\bullet \tag{10}$$

$$\eta_{ORC} = \frac{W_{net}^\bullet}{Q_{Evap}^\bullet} \tag{11}$$

3.2. Desiccant Cooling System (DCS)

The desiccant wheel is the main component of the DCS, and the model established by Panaras et al. [25] is used to simulate the desiccant wheel in this study. The following are the associated energy balances and governing equations for the DCS components:

- The combined potential of the desiccant wheel

$$F_{1,i} = \left[-\frac{2865}{(t_i + 273.15)^{1.49}} \right] + 4.344 [w_i / 1000]^{0.8624} \tag{12}$$

$$F_{2,i} = \left[\frac{(t_i + 273.15)^{1.49}}{6360} \right] - 1.127 [w_i / 1000]^{0.07969} \tag{13}$$

- Desiccant wheel's efficiency

$$\eta_{F1} = \frac{F_{1,2} - F_{1,1}}{F_{1,8} - F_{1,1}} \tag{14}$$

$$\eta_{F2} = \frac{F_{2,2} - F_{2,1}}{F_{2,8} - F_{2,1}} \tag{15}$$

- Energy and mass balances of the desiccant wheel

$$m_{P,a}^\bullet (h_{a2} - h_{a1}) = m_{R,a}^\bullet (h_{a8} - h_{a9}) \tag{16}$$

$$m_{P,a}^\bullet (w_{a1} - w_{a2}) = m_{R,a}^\bullet (w_{a9} - w_{a8}) \tag{17}$$

- Heat exchanger

$$m_{P,a}^\bullet c_{p,ma} (t_{a2} - t_{a3}) = m_{R,a}^\bullet c_{p,ma} (t_{a7} - t_{a6}) \tag{18}$$

$$\epsilon_{HE-1} = \frac{m_{P,a}^\bullet c_{p,ma} (t_{a2} - t_{a3})}{C (t_{a2} - t_{a6})_{min}} \tag{19}$$

where,

$$C_{min} = \min \{ m_{P,a}^\bullet c_{p,ma}, m_{R,a}^\bullet c_{p,ma} \}$$

- Direct evaporative coolers:

$$\eta_{DEC-1} = \frac{t_{a3} - t_{a4}}{t_{a3} - t_{a3,wb}} \tag{20}$$

$$\eta_{DEC-1} = \frac{w_{a4} - w_{a3}}{w_{a4,ideal} - w_{a3}} \tag{21}$$

$$\eta_{DEC-2} = \frac{t_{a5} - t_{a6}}{t_{a5} - t_{a5,wb}} \tag{22}$$

$$\eta_{DEC-2} = \frac{w_{a6} - w_{a5}}{w_{a6,ideal} - w_{a5}} \tag{23}$$

- Regeneration energy, space cooling capacity and coefficient of performance

$$Q_{in,DCS}^{\bullet} = m_{R,a}^{\bullet}(h_{a8} - h_{a7}) \tag{24}$$

$$Q_{cooling}^{\bullet} = m_{P,a}^{\bullet}(h_{a5} - h_{a4}) \tag{25}$$

$$COP_{DCS} = \frac{Q_{cooling}^{\bullet}}{Q_{in,DCS}^{\bullet}} \tag{26}$$

3.3. Humidification Dehumidification Water Desalination System (HDH)

The energy balance of the humidifier [20] is given as

$$m_{R,a}^{\bullet}(h_{a10} - h_{a9}) = m_w^{\bullet}h_{w3} - m_{brine}^{\bullet}h_{w4} \text{ (for MGS - I \& MGS - II)} \tag{27}$$

where,

$$m_{brine}^{\bullet} = m_w^{\bullet} - m_{makeup}^{\bullet}$$

The mass flow rate of the makeup water (sea or brackish water) supplied to the system [20] is given as

$$m_{makeup}^{\bullet} = m_{R,a}^{\bullet}(w_{a10} - w_{a9}) \tag{28}$$

The energy balance and freshwater productivity of the first dehumidifier in the basic system [20] are given as

$$m_{R,a}^{\bullet}(h_{a10} - h_{a11}) = m_w^{\bullet}(h_{w2} - h_{w1}) + m_{fresh}^{\bullet}h_{w5} \tag{29}$$

$$\epsilon_{deh-1} = \frac{m_w^{\bullet}c_{p,w}(t_{w2} - t_{w1})}{C(t_{a10} - t_{w1})_{min}} \tag{30}$$

$$m_{fresh}^{\bullet}(MGS - I) = m_{R,a}^{\bullet}(w_{a10} - w_{a11}) \tag{31}$$

where,

$$h_{w5} = c_{p,w}t_{a11}$$

$$C_{min} = \min\{m_w^{\bullet}c_{p,w}, m_{R,a}^{\bullet}c_{p,ma}\}$$

The energy balance, freshwater productivity of the second dehumidifier, and total freshwater productivity for MGS-II systems [20] are given as

$$m_{R,a}^{\bullet}(h_{a11} - h_{a12}) = m_w^{\bullet}(h_{w10} - h_{w1}) + m_{fresh-II}^{\bullet}h_{w6} \tag{32}$$

$$m_{fresh,II}^{\bullet} = m_{R,a}^{\bullet}(w_{a11} - w_{a12}) \tag{33}$$

$$m_{fresh}^{\bullet}(MGS - II) = m_{fresh}^{\bullet}(MGS - I) + m_{fresh,II}^{\bullet} \tag{34}$$

The gain output ratio (GOR) for MGS-I and MGS-II systems [20] is given by

$$GOR_{HDH}(MGS - I) = \frac{m_{fresh}^{\bullet}(MGS - I)h_{fg}}{m_w^{\bullet}(h_{w3} - h_{w2}) + m_{R,a}^{\bullet}(h_{a9} - h_{a1})} \tag{35}$$

$$GOR_{HDH}(MGS - II) = \frac{m_{fresh}^{\bullet}(MGS - II)h_{fg}}{m_w^{\bullet}(h_{w3} - h_{w2}) + m_{R,a}^{\bullet}(h_{a9} - h_{a1})} \tag{36}$$

3.4. Hot Water for Domestic Application in MGS-II

$$\varepsilon_{HE-3} = \frac{Q_{heating-I}^{\bullet}}{m_{brine}^{\bullet}c_{p,w}(t_{w4} - t_{s5})} \tag{37}$$

$$\varepsilon_{HE-4} = \frac{Q_{heating-II}^{\bullet}}{m_{fresh}^{\bullet}(MGS - II)c_{p,w}(t_{w8} - t_{s5})} \tag{38}$$

$$Q_{heating}^{\bullet} = Q_{heating-I}^{\bullet} + Q_{heating-II}^{\bullet} \tag{39}$$

$$m_{fresh}^{\bullet}(MGS - II)c_{p,w}t_{w8} = m_{fresh}^{\bullet}(MGS - I)c_{p,w}t_{w7} + m_{fresh,II}^{\bullet}c_{p,w}t_{w6} \tag{40}$$

3.5. System Performance Parameters and Evaluation

The tri-generation total gained output ratio (TGOR), tri-generation gained output ratio for independent systems (TGOR_{Rind}), specific total gained energy (STG), and specific total gained energy equivalent price (STGP) of the proposed basic, IS-I, and IS-II multi-generation systems [20] are as follows.

$$TGOR_{MGS-I} = \frac{m_{fresh}^{\bullet}(MGS - I)h_{fg} + Q_{cooling}^{\bullet} + W_{net}^{\bullet}}{Q_{Evap}^{\bullet}} \tag{41}$$

$$TGOR_{MGS-II} = \frac{m_{fresh}^{\bullet}(MGS - II)h_{fg} + Q_{Domes}^{\bullet} + Q_{cooling}^{\bullet} + W_{net}^{\bullet}}{Q_{Evap}^{\bullet}} \tag{42}$$

$$STG_{MGS-I} = \frac{(m_{fresh}^{\bullet}(MGS - I)h_{fg} + Q_{cooling}^{\bullet} + W_{net}^{\bullet})\Delta\tau}{A_{SC}} \tag{43}$$

$$STG_{MGS-II} = \frac{(m_{fresh}^{\bullet}(MGS - II)h_{fg} + Q_{heating}^{\bullet} + Q_{cooling}^{\bullet} + W_{net}^{\bullet})\Delta\tau}{A_{SC}} \tag{44}$$

$$STGP_{MGS-I} = [m_{fresh}^{\bullet}(MGS - I) \times WUR + (Q_{cooling}^{\bullet} + W_{net}^{\bullet}) \times EUR] \Delta\tau \tag{45}$$

$$STGP_{MGS-II} = [m_{fresh}^{\bullet}(MGS - II) \times WUR + (Q_{Domes}^{\bullet} + Q_{cooling}^{\bullet} + W_{net}^{\bullet}) \times EUR] \Delta\tau \tag{46}$$

where,

$\Delta\tau$: daylight time (12 h)

WUR: water unit rate USD/kg

EUR: Energy unit rate USD/kWh

The prices for energy and freshwater units vary from one city to another. In the present study, typical values of energy and water unit prices of 0.05 USD/kWh and 2.5 USD/m³ of Gulf cities [8,28] are taken. The system governing equations (Equations (1)–(46)) are simulated by using C++ and EES software based on energy and mass balances for all system components to calculate the system performance and productivity parameters for different ranges of design and operating conditions as given in Table 1.

4. Results and Discussion

The thermodynamics analysis was carried out to assess the performance of proposed multi-generation systems (MGS-I and MGS-II) for electricity production, freshwater and space cooling, and domestic heating through the integration of solar ORC with DCS and HDH subsystems. The effects of the controlling parameters (Δt_{sup} , t_{f1} , t_{w1} , and MR) on

the systems' productivities ($\dot{W}_{net}, \dot{m}_{fresh}, \dot{Q}_{cooling}/\dot{Q}_{cooling}$) and the system's performance indicators ($\eta_{ORC}, GOR_{HDH}, COP_{DCS}, TGOR, STG,$ and $STGP$) are investigated, discussed, and evaluated using n-Octane as an organic fluid.

4.1. Model Validation

To confirm the developed thermodynamic models in the present study, model validation is implemented, and the results of the current work are compared with those reported in the literature to determine their degree of accuracy. Table 3 illustrates the validation of the current thermodynamic models with previously published data in [28–30] for the HDH, ORC, and DCS subsystems. In Table 3, a good agreement is observed between the results obtained in the current work and those reported previously in the literature.

Table 3. Validation of the current model with the published data for HDH, ORC, and DCS systems.

$m^{\bullet}_w/m^{\bullet}_a$ (kg_w/kg_a)	HDH		P_{evap} [bar]	ORC		T_{reg} [°C]	DCS	
	GOR_{HDH}			η_{ORC}			COP_{DCS}	
	Exp. Zubair et al. [29]	Num. Current model		Exp. Galloni et al. [30]	Num. Current model		Exp. Panaras et al. [25]	Num. Current model
1.36	0.335	0.325	6.180	6.313	5.842	50	0.387	0.402
			6.897	6.347	6.35			
			7.906	5.241	6.96			
1.89	0.365	0.375	8.806	8.150	7.423	60	0.412	0.431
			9.587	8.981	7.777			
2.27	0.375	0.387	9.955	8.889	7.931	70	0.443	0.470

4.2. Systems' Productivities

The influences of operating parameters ($\Delta t_{sup}, t_{f1}, t_{w1},$ and MR) on the systems' productivities; electrical power generation, freshwater productivity (\dot{m}_{fresh}), space cooling capacity ($\dot{Q}_{cooling}$), domestic heating capacity ($\dot{Q}_{heating}$), of the proposed multi-generation systems (MGS-I and MGS-II) are presented in Table 4 and Figures 3 and 4. Table 4 and Figures 3a and 4b,d demonstrate the effect of the superheat degree, Δt_{sup} , on the $\dot{W}_{net}, \dot{m}_{fresh}, \dot{Q}_{cooling}$ and $\dot{Q}_{heating}$ at $t_{f1} = 50\text{ }^{\circ}\text{C}, t_{w1} = 20\text{ }^{\circ}\text{C},$ and $MR = 0.25$. As shown in Figure 3a, Figure 4b and Table 4, the values of $\dot{W}_{net}, \dot{Q}_{cooling}, \dot{m}_{fresh},$ and $\dot{Q}_{heating}$ improve with increasing Δt_{sup} . Such a trend is the same for the proposed systems (MGS-I and MGS-II). This is attributed to the increase in turbine work, solar energy needed, and the heat liberated at the ORC condenser as the turbine inlet temperature increases. This reflects the increase in the needed area of solar collectors, air humidification capacity inside the humidifier, space cooling capacity, and domestic heating capacity.

Table 4. Power, ORC thermal efficiency, and area of solar collectors for MGS-I and MGS-II.

Δt_{sup} (°C)	t_{f1} (°C)	t_{w1} (°C)	MR	W^{\bullet}_{net} (kW)	η_{ORC} (%)	A_{solar} (m ²)
0	50	20	0.25	79.89	14.85	1064
20	50	20	0.25	84.37	14.44	1155
45	50	20	0.25	89.89	13.96	1273
45	40	20	0.25	102.3	15.34	1319
45	50	20	0.25	89.89	13.96	1273
45	60	20	0.25	78.23	12.61	1227
45	50	15	0.25	89.89	13.96	1273
45	50	20	0.25	89.89	13.96	1273
45	50	25	0.25	89.89	13.96	1273
45	50	20	0.1	89.89	13.96	1273
45	50	20	0.25	89.89	13.96	1273
45	50	20	0.4	89.89	13.96	1273

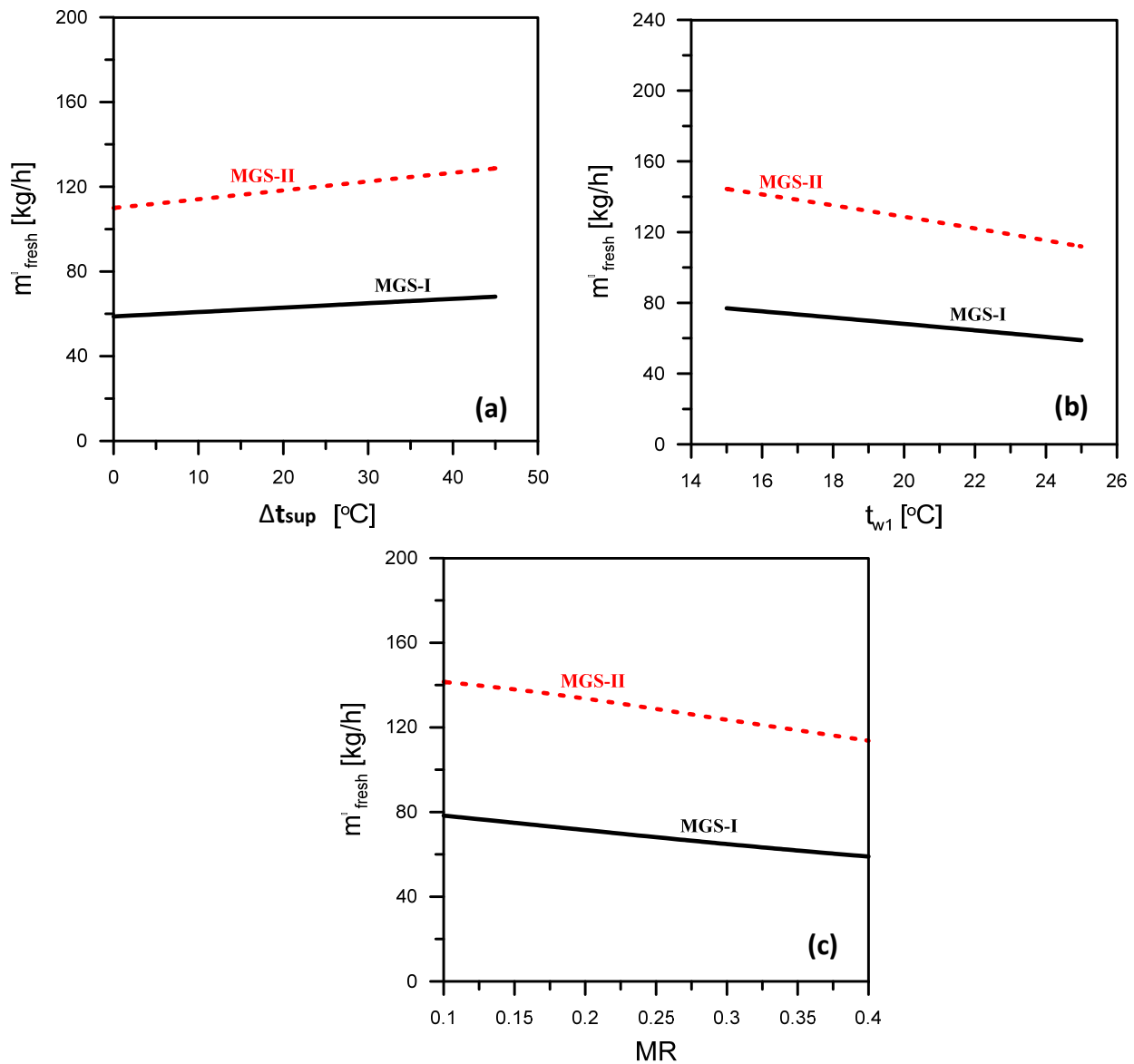


Figure 3. Impact of studied parameters on freshwater: (a) Δt_{sup} ; (b) t_{w1} (c) \dot{m}_{fresh} .

Moreover, Table 4 displays the effect of $tf1$ on the systems' productivities at $\Delta t_{sup} = 45$ °C, $t_{w1} = 20$ °C, and $MR = 0.25$. The condensing temperature of ORC harms the \dot{W}_{net} , \dot{m}_{fresh} , $\dot{Q}_{cooling}$. Such a trend is similar for MGS-I and MGS-II. Increasing the condensation temperature reduces the turbine power due to the reduction in enthalpy difference across the turbine, which also results in a decreasing freshwater rate. This is a result of reducing the heat recovered from the condenser to water and air streams before entering the humidifier, which reduces the amount of water evaporation and consequently reduces the dehumidifier capacity. In addition, increasing the condenser pressure reduces the regeneration temperature of DCS, which, in turn, causes a reduction in space cooling capacity.

Furthermore, Figure 3b and Table 4 show that increasing t_{w1} has an adverse and negligible effect on \dot{m}_{fresh} and \dot{W}_{net} , respectively. Decreasing \dot{m}_{fresh} is due to decreasing the air dehumidification capacity through the dehumidifier, which leads to a lower freshwater production rate. Nevertheless, the increase in water inlet temperature has no impact on \dot{W}_{net} (see Table 4). This is because of the independence of the ORC heat supply and liberated to the seawater inlet temperature.

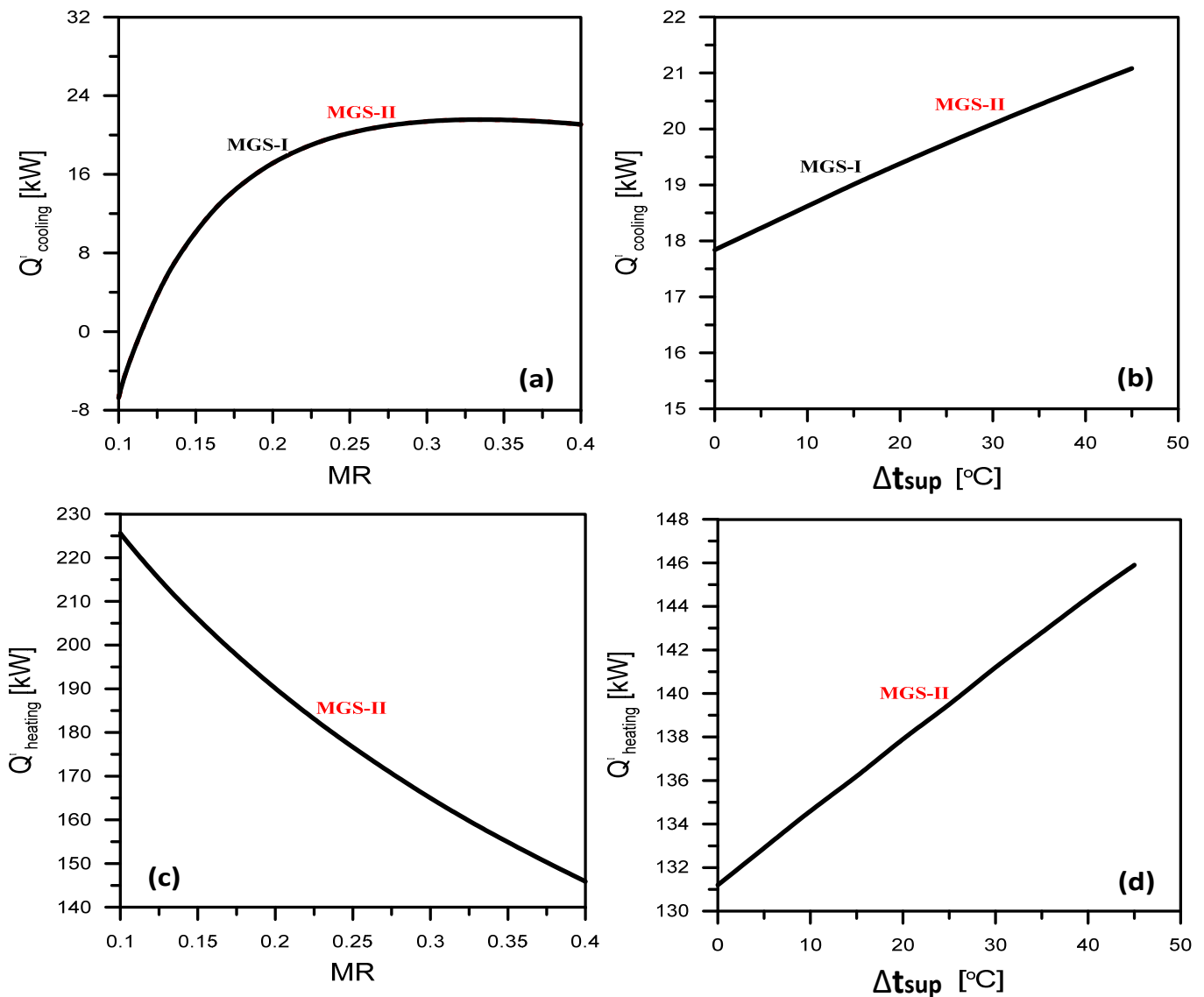


Figure 4. Impact of studied parameters on space cooling and domestic heating: (a) MR on $\dot{Q}_{cooling}$; (b) Δt_{sup} on $\dot{Q}_{cooling}$; (c) MR on $\dot{Q}_{heating}$; (d) Δt_{sup} on $\dot{Q}_{heating}$.

Figures 3c and 4a,c and Table 4 show the effects of MR on the \dot{W}_{net} , \dot{m}_{fresh} , $\dot{Q}_{cooling}$ and $\dot{Q}_{heating}$. Increasing MR has adverse impacts on \dot{m}_{fresh} and $\dot{Q}_{heating}$ due to the decrease in evaporation rate in the humidifier due to reducing the seawater flow rate with increasing MR. This results in a lower freshwater yield and domestic heating capacity. Figure 4a displays the increase of $\dot{Q}_{cooling}$ with increasing MR until it attains a maximum value and then starts to drop with increasing MR. Increasing MR has two opposing effects: it reduces air flow rate and increases the enthalpy difference across the conditioned space. In the first interval of MR, the increase in enthalpy difference across the space dominates the reduction in air mass flow rate, which leads to improved $\dot{Q}_{cooling}$ and vice versa in the second interval of MR. Table 4 also shows that MR does not affect on \dot{W}_{net} and that this is because the ORC heat source and rejected heat are independent of MR. Comparing the proposed multi-generation systems (MGS-I and MGS-II), Figure 4a–c shows that the freshwater productivity of the MGS-II system is higher than that of the MGS-I system. The trend is consistent across all Δt_{sup} , $tf1$, $tw1$, and MR values. This is due to adding a second stage to the dehumidifier of the MGS-II system.

The space cooling of the three proposed systems is shown in Figure 4a,b. The space cooling capacity of both the MGS-II and MGS-I systems show similar space cooling capacities. Such a trend is the same at any Δt_{sup} , $tf1$, $tw1$, or MR . This is a result of the regeneration heat recovery for DCS not affected by the improvements applied to the MGS-II system (i.e., second stage dehumidification, brine and freshwater heat recovery at HE-3 and HE-4, respectively). The proposed multi-generation systems produce the same turbine power (see Table 3). Such a trend is the same at any Δt_{sup} , $tf1$, $tw1$, or MR . The improvements of the MGS-II system are not affected by the turbine power compared to the MGS-I system (i.e., adding second stage dehumidification and brine and freshwater heat recovery). As shown in Figure 3, Figure 4 and Table 4, for the MGS-II system, the maximum system productivity of \dot{W}_{net} , \dot{m}_{fresh} , $\dot{Q}_{cooling}$, and $\dot{Q}_{heating}$ and are 102.3 kw, 142 kg/h, 22 kW and 225 kW, respectively.

4.3. Systems' Performance

The effects of operating parameters (Δt_{sup} , $tf1$, $tw1$, and MR) on the systems' performance indicators (η_{ORC} , GOR_{HDH} , COP_{DCS} , $TGOR$, STG , $STGP$) of the three proposed multi-generation systems (MGS-I and MGS-II) are given in Table 4 and Figures 5–8. Systems' performance indicators for the proposed systems at operating conditions of $tf1 = 50$ °C, $tw1 = 20$ °C, and $MR = 0.25$ are slightly decreased with increasing Δt_{sup} . Heat input to ORC, HDH, and DCS increases with increasing turbine inlet temperature, which results in a drop in η_{ORC} , GOR_{HDH} , and consequently lower $TGOR$, STG , and $STGP$, for MGS-I and MGS-II proposed systems, the solar area, A_{solar} , increases as Δt_{sup} increases (see Table 4). Increasing the amount of superheat at the turbine inlet requires increasing the solar input heat of the ORC.

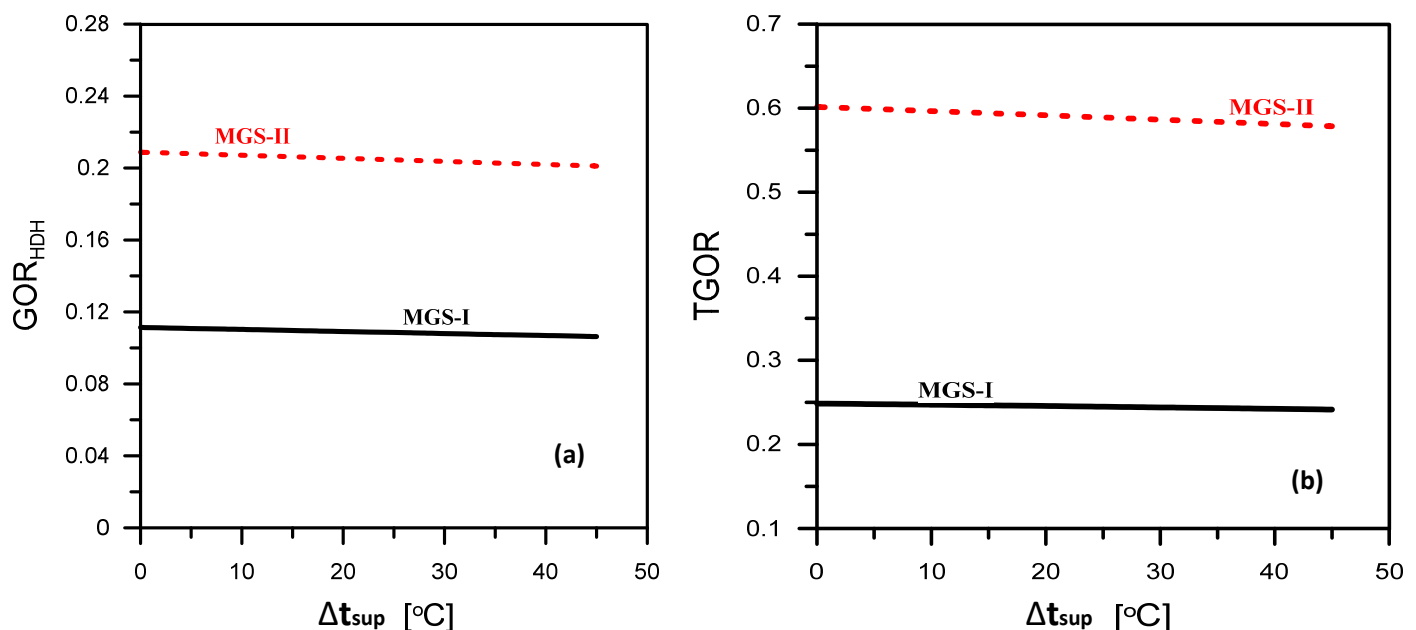


Figure 5. Impact of ORC superheat degree on the proposed systems' performance: (a) GOR_{HDH} ; (b) $TGOR$.

A comparison between the proposed multi-generation systems, Figure 5a, b shows that the system performance parameters (GOR_{HDH} , $TGOR$) of the MGS-II system are higher than those of the MGS-I system. Such a trend is the same at any Δt_{sup} . Improving $TGOR$, STG , and $STGP$ of the MGS-II system rather than the MGS-I system is attributed to the increase in total output system energy due to brine and freshwater heat recovery. This heat recovery increases heating capacity in domestic applications ($\dot{Q}_{heating}$), which improves the

TGOR of MGS-II rather than MGS-I and consequently improves the STG and STGP. The MGS-II system has better GOR_{HDH} than that of the MGS-I. System.

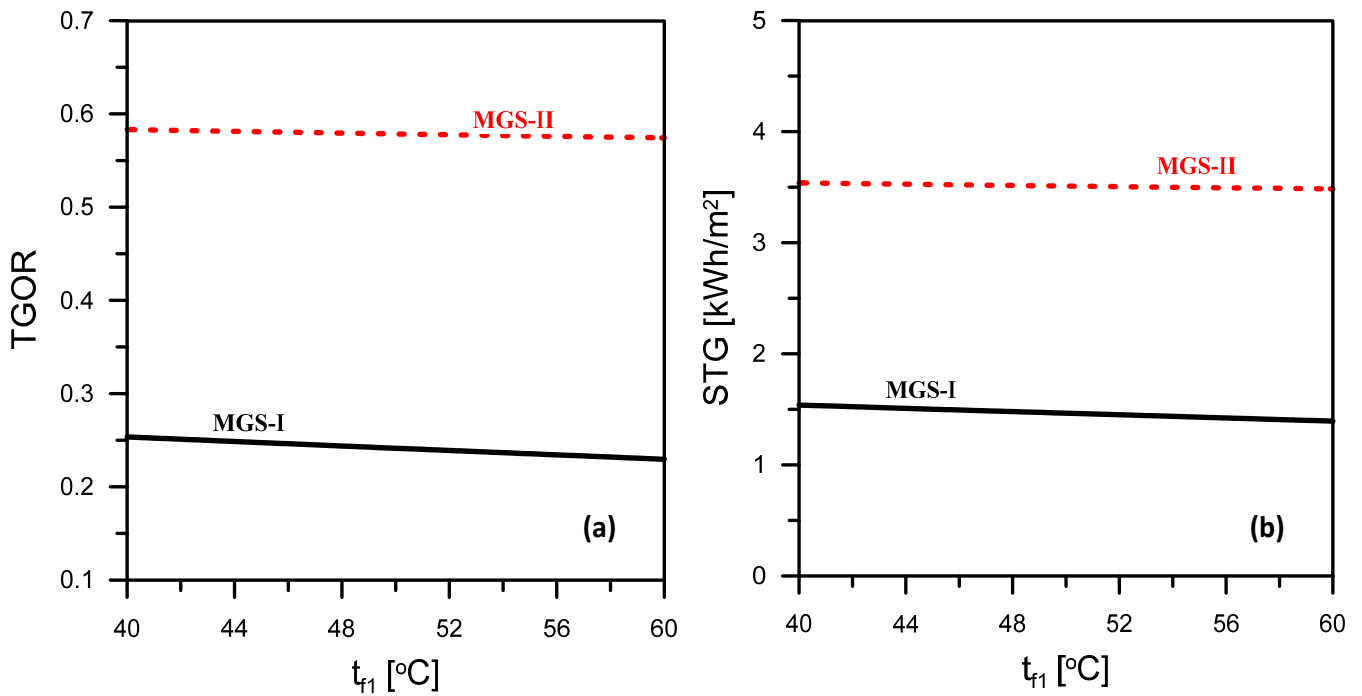


Figure 6. Impact of ORC condensation temperature on proposed systems' performance: (a) TGOR; (b) STG.

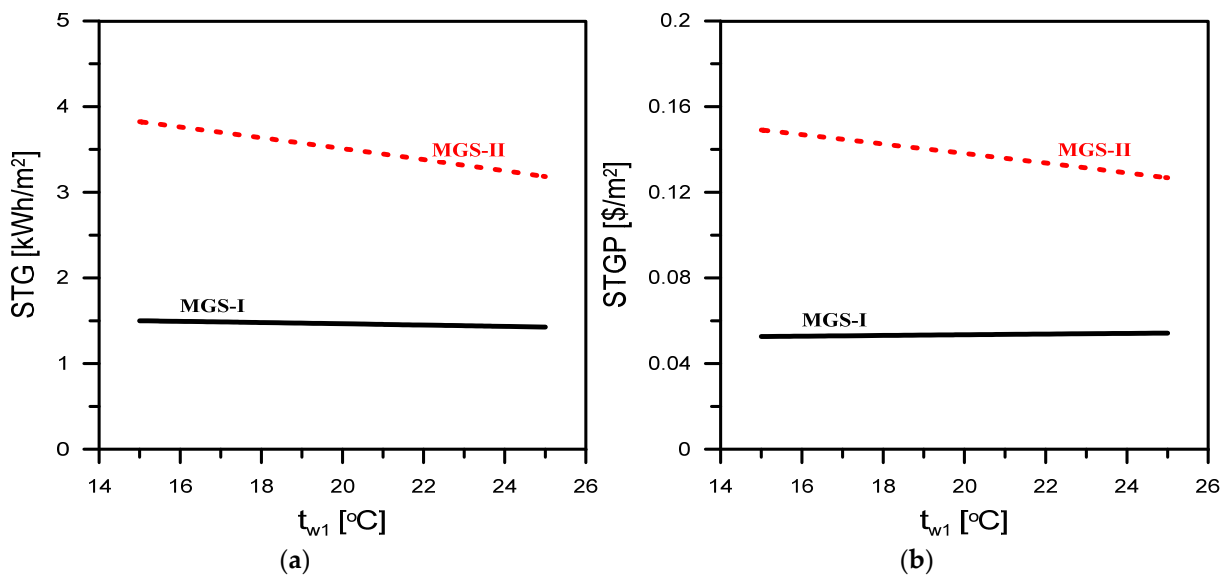


Figure 7. Impact of seawater inlet temperature on proposed systems' performance: (a) STG; (b) STGP.

Table 4 and Figure 6a,b show the values of the system performance indicators η_{ORC} , TGOR, and STG at operating temperatures of $\Delta t_{sup} = 45$ °C, $t_{w1} = 20$ °C, and $MR = 0.25$. All performance parameters are slightly decreased with increasing t_{f1} . Such a trend is the same for the proposed systems. The decrease in η_{ORC} with the increase in condensation temperature (see Table 4) is due to the reduction in enthalpy difference across the turbine with the same heat energy input. While the reduction of TGOR and STG is attributed to the increase in the amount of input heat energy to HDH and DCS. Increasing the t_{f1}

leads to a reduction in TGOR and STG. Solar area, A_{solar} , decreases with increasing $tf1$ (see Table 4) for all proposed systems. This is because of reducing the required solar input heat to the ORC with increased condensation temperature. When comparing the proposed multi-generation systems, the MGS-II system has a higher performance than the MGS-I systems. This is attributed to the increase in total output system energy as a result of brine and freshwater heat recovery used for \dot{Q}_{heating} .

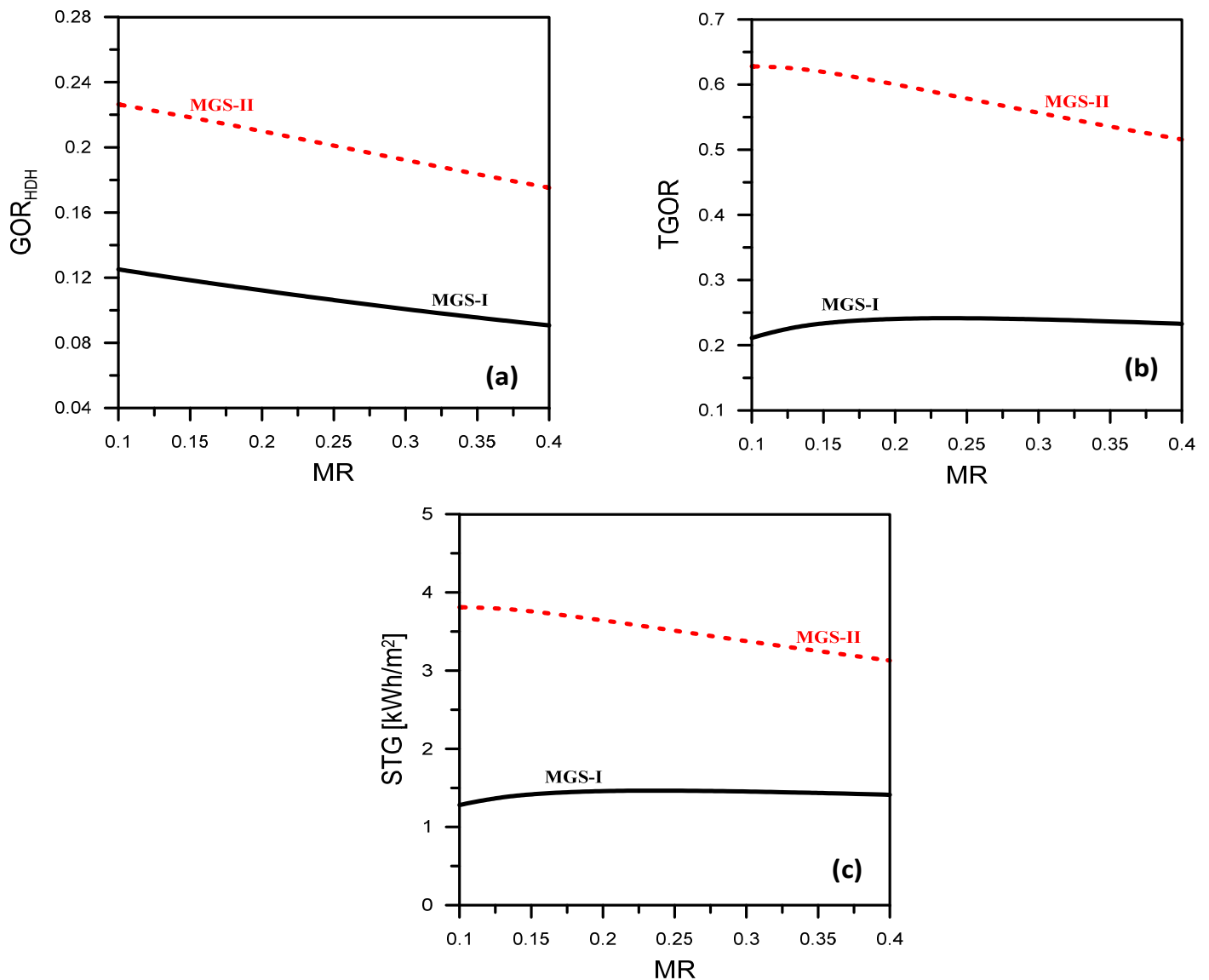


Figure 8. Impact of mass flow rate ratio on proposed systems' performance: (a) GOR_{HDH} ; (b) TGOR; (c) STG.

The effect of seawater temperature, $tw1$, on systems' performance indicators is also shown in Figure 7 and Table 4 at $\Delta t_{\text{sup}} = 45$ °C, $tf1 = 50$ °C, and $MR = 0.25$. As shown in Figure 7a,b, the STG and STGP decrease as $tw1$ increases. Such a trend is the same for proposed systems. The increase in the water inlet temperature has no impact on the η_{ORC} and A_{solar} (see Table 4). This is because of the independence of the solar heat source of the ORC and the heat liberated to the seawater inlet temperature. Similarly, comparing the two proposed multi-generation systems, Figure 7a,b show that the MGS-II system has the best system performance among the three systems within the studied range of $tw1$.

The influence of mass flow rate ratio, MR, on the systems' performance indicators is displayed in Figure 8 and Table 4 at $\Delta t_{sup} = 45\text{ }^\circ\text{C}$, $t_{f1} = 50\text{ }^\circ\text{C}$, and $t_{w1} = 20\text{ }^\circ\text{C}$. As shown in Figure 8a–c, the performance indicators (GOR_{HDH} , TGOR and STG) declined with increasing MR for the two proposed systems. Increasing MR, as a result of decreasing both air and seawater mass flow rates, with fixed \dot{m}_{ORC} leads to a lower rate of evaporation in the humidifier and, consequently, a lower rate of condensation in the dehumidifier. Hence, lower values of GOR_{HDH} are obtained, as shown in Figure 8a. Moreover, increasing MR has no impact on the η_{ORC} and A_{solar} (see Table 4). In other words, it becomes independent of the solar heat source of ORC and the heat liberated to the seawater inlet temperature. In addition, Figure 8a–c show that the MGS-II system has the best performance rather to the MGS-I system within the studied range of MR. As shown in Figures 5–8 and Table 4, The maximum GOR_{HDH} , η_{ORC} , A_{solar} , TGOR, STG, and STGP of the MGS-II system within the ranges of all studied parameters are 0.21, 15.34 %, 1273 m^2 , 0.6303, 3.824 kWh/m^2 , and 0.149 USD/m^2 , respectively.

4.4. Maximum Proposed Systems' Productivity

In light of previous discussions, the evaluation of the currently proposed systems will be based on the number of needed productivities (electrical power, fresh water, and cooling/heating capacity). Figure 9a–c shows comparisons of the two proposed systems (MGS-I and MGS-II) at the maximum systems' productivity under the same operating conditions. The maximum \dot{W}_{net} , \dot{m}_{fresh} , $\dot{Q}_{cooling}$ within the ranges of all studied parameters are 102.3 kW (MGS-I and MGS-II), 141.5 kg/h (MGS-II), and 20.77 kW (MGS-I and MGS-II), respectively.

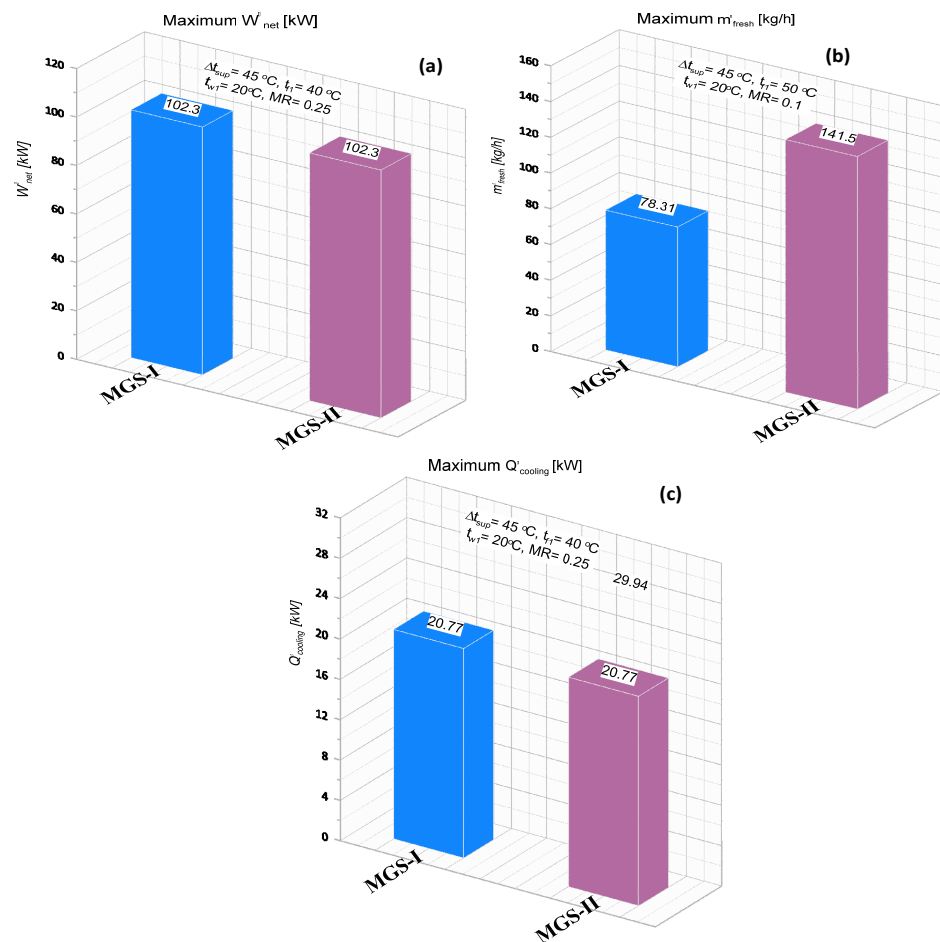


Figure 9. Comparisons of maximum proposed systems' productivity and performance: (a) \dot{W}_{net} ; (b) \dot{m}_{fresh} ; (c) $\dot{Q}_{cooling}$.

Correspondingly, systems evaluation can also be measured by space-supplied air conditions (ta_4 and wa_4) to maintain human comfort conditions inside the conditioned space. Figure 10 illustrates all available air-conditioned space supply conditions on the psychrometric charts for all studied parameter ranges relative to the space condition ($25\text{ }^\circ\text{C}$ and 12 gv/kga). The accepted conditions of space-supplied air are shown in the figures to be $ta_4 = 15.5\text{--}18.2\text{ }^\circ\text{C}$ and $wa_4 = 9.2\text{--}12.00\text{ gv/kga}$ for systems MGS-I and MGS-II. Otherwise, the conditions outside are not desirable.

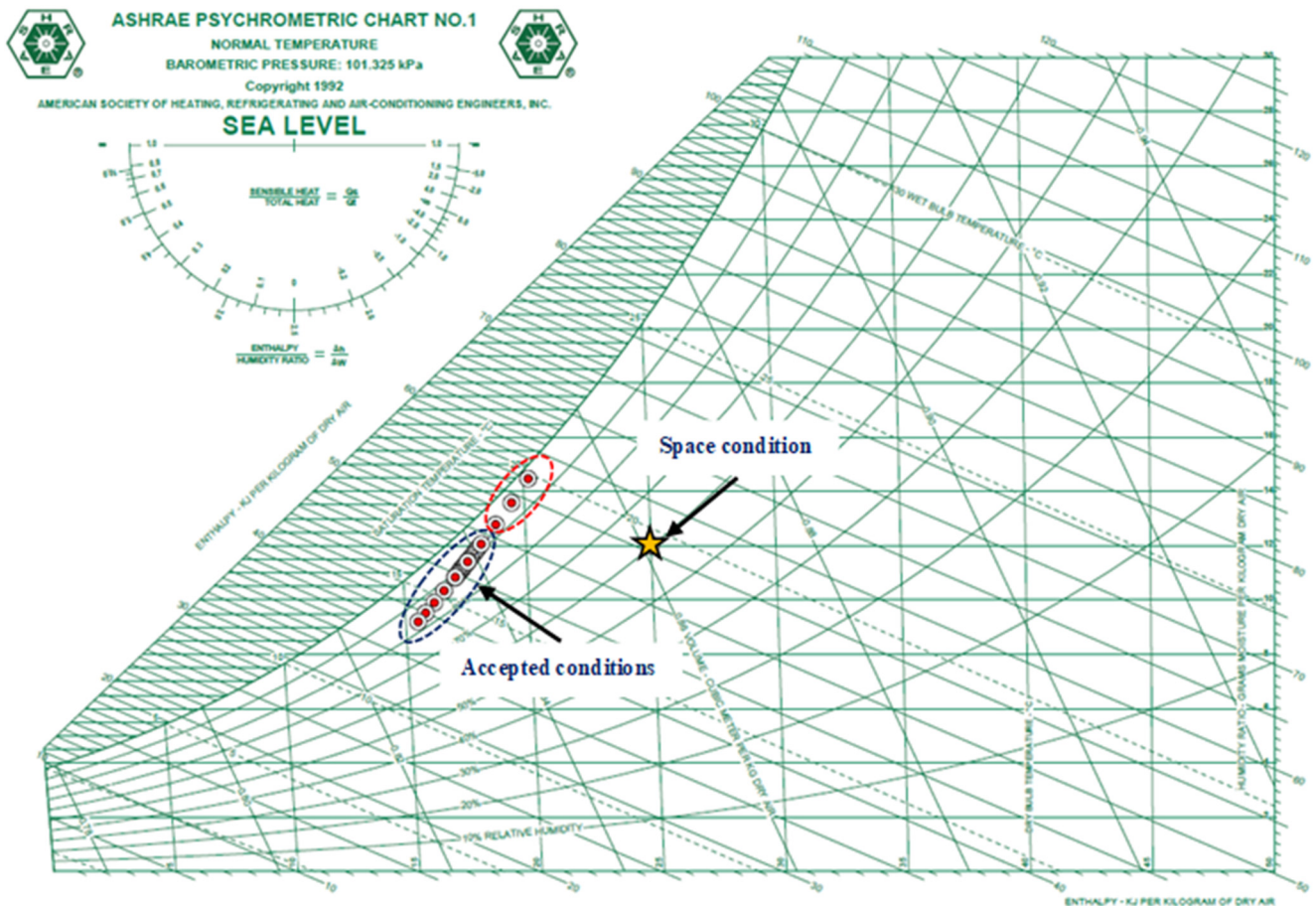


Figure 10. Accepted supply conditions to air-conditioned space (systems evaluation) for MGS-I and MGS-II.

Figure 11a shows the limits of supplied conditions (ta_4 and wa_4) of conditioned space for two proposed systems (MGS-I and MGS-II) at any \dot{W}_{net} for all studied parameter ranges. Moreover, Figure 11b displays the values and limitations of \dot{W}_{net} and $\dot{Q}_{cooling}$ at any \dot{m}_{fresh} for two systems and all studied parameter ranges. Figure 11 can help researchers, solar multi-generation developers, power plant designers, and investors relate the proposed systems' productivities (electricity, space cooling, freshwater) in the design stage to select the suitable multi-generation system based on the needed application.

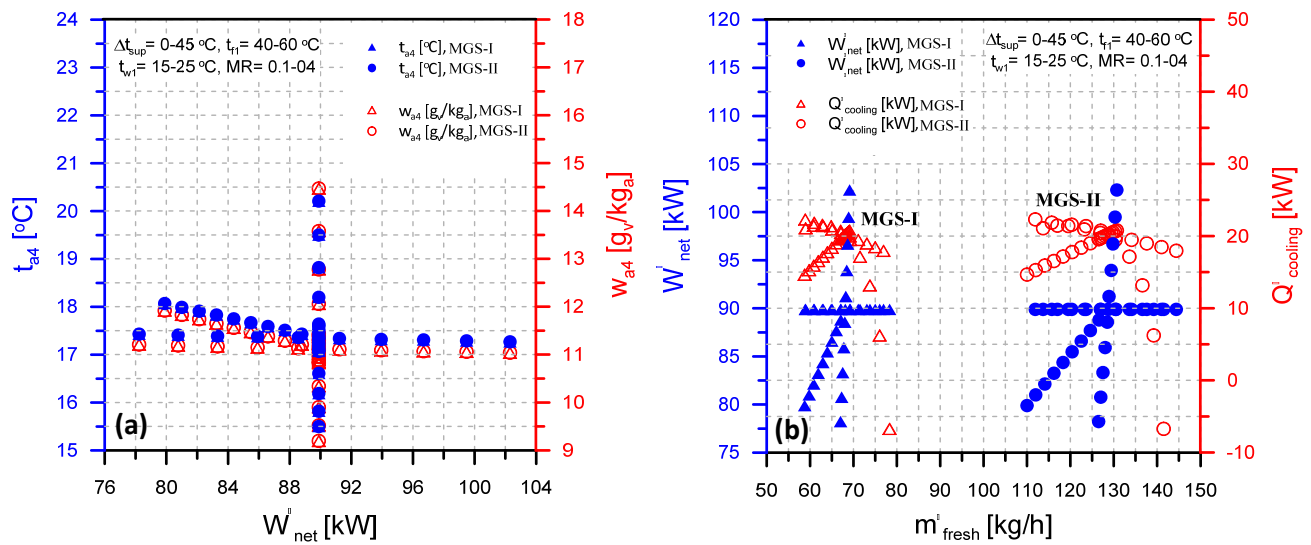


Figure 11. System assessment and evaluation: (a) Space-supplied air conditions versus produced fresh water rate, (b) power output and space cooling capacity versus produced fresh water rate.

4.5. Comparisons with Other Reported Systems

For more contribution and to prove the current proposed systems' capability, reliability, applicability, and practical use the current systems' results are compared with the related results in other published works. The maximum TGOR and maximum freshwater productivity of co-generation and tri-generation systems are chosen as performance and productivity indicators for comparison to the currently proposed systems. However, they differ in operating conditions from our chosen conditions, as shown in Table 5. As shown in Table 5, the current system (MGS-II) has maximum TGOR and freshwater productivity better than the comparable systems.

Table 5. Comparison of the current systems with other reported systems.

Refs	System Type	System Productivities	Prime Mover	Application	Study Description	Max. Fresh Water Productivity (kg/h)	TGOR _{max} / η_{max}
Tehrani et al. [31]	co-generation	Heating/Power	Gas turbine combined cycle	Industrial	Modeling	—	59.96%
Choi et al. [32]	tri-generation	Cooling/Heating/Power	gas turbine vapor compression refrigeration cycle	Commercial	Modeling	—	53.3%
Fouda et al. [33]	co-generation	Cooling/Fresh water	Internal combustion engine	Residential	Modeling	21.5	—
Puig-Arnabat et al. [34]	tri-generation	Cooling/Heating/Power	SOFC/ORC combined	Commercial	Modeling	—	64.2%
Al-Sulaiman et al. [35]	tri-generation	Cooling/Heating/Power	ORC	Commercial	Modeling	—	74%
Huang et al. [36]	tri-generation	Cooling/Heating/Power	vapor compression refrigeration cycle	Commercial	Modeling	—	71.7%
Nada et al. [37]	co-generation	Cooling/Fresh water	Solar/Rankine cycle	Residential	Experimental	17.42	—
Abdelhay et al. [16]	tri-generation	electricity, cooling, and potable water	Solar/ORC combined	Residential	Modeling	22.9	—
Fouda et al. [20]	tri-generation	electricity, cooling, and potable water	Solar/ORC combined	Residential	Modeling	72.37	26.43 %
Current systems	Multigeneration	Cooling/Heating/Power/Fresh water	Solar/ORC combined	Residential	Modeling	141.5 (MGS-II)	63.03% (MGS-II)

5. Conclusions

Thermodynamics analysis of a more efficient novel solar-driven multi-generation system (MGS-II) combined with ORC, HDH, and DCS with heat recovery systems have

been investigated and presented for producing electricity, space cooling/domestic heating, and freshwater production. The effect of different system operating and design parameters on the systems' productivities and performance indicators was studied. In addition, a comparison study with the basic multi-generation system (MGS-I) is performed. Moreover, the validated system models have been applied to the performance evaluation when operating conditions are varied. Consequently, the following conclusions can be drawn:

- The proposed multi-generation systems can produce electricity, fresh water, and cooling/domestic heating while maintaining human thermal comfort conditions inside the buildings.
- The \dot{W}_{net} , \dot{m}_{fresh} and $\dot{Q}_{cooling}$ for all systems improve with increasing Δt_{sup} and decrease with increasing ORC condensing temperature, while $tw1$ has an adverse, positive, and negligible effect on \dot{m}_{fresh} , $\dot{Q}_{cooling}$, and \dot{W}_{net} , respectively.
- The \dot{m}_{fresh} drops with increasing MR, while $\dot{Q}_{cooling}$ improves with increasing MR until it reaches a maximum value and decreases with increasing MR.
- MGS-II system has higher GOR_{HDH} , TGOR, STG, and STGP than the MGS-I system.
- GOR_{HDH} , TGOR, STG, and STGP for two proposed systems drop with increasing $tw1$.
- $\dot{Q}_{cooling}$ improves with an increase in MR until they reach peak values, decreasing considerably.
- The accepted ranges of systems input studied parameter were determine based on the accepted ranges comfortable space-supplied air conditions (temperature and humidity) at $t_{a4} = 15.5\text{--}18.2\text{ }^{\circ}\text{C}$ and $w_{a4} = 9.2\text{--}12.00\text{ gv/kga}$ for systems MGS-I and MGS-II. Otherwise, the conditions outside are not desirable.
- The maximum \dot{W}_{net} , \dot{m}_{fresh} , $\dot{Q}_{cooling}$ within the ranges of all studied parameters are 102.3 kW (MGS-I and MGS-II), 141.5 kg/h (MGS-II), and 20.77 kW (MGS-I and MGS-II), respectively.
- Charts with limitations of \dot{W}_{net} , $\dot{Q}_{cooling}$ at any \dot{m}_{fresh} for studied systems within all studied parameter ranges are presented.
- The maximum GOR_{HDH} , η_{ORC} , A_{solar} , TGOR, STG, and STGP of the MGS-II system within the ranges of all studied parameters are 0.21, 15.34 %, 1273 m², 0.6303, 3.824 kWh/m², and 0.149 USD/m², respectively.
- The current system (MGS-II) has the maximum of the system's performance indicators and productivity (TGOR and \dot{m}_{fresh}) compared with the related systems
- Finally, we acknowledge that the current work presented in this paper is just a start for poly-generation systems; using different improvements of ORC, types of A/C (adsorption and absorption) and desalination (RO, MED) systems in addition to transient analysis are recommended as a future work for poly-generation systems.

Author Contributions: H.F.E.: Management and coordination responsibility for the research activity planning and execution, Conceptualization, methodology, Data collection, Writing—Original draft preparation, Manuscript preparation and data analysis, visualization. A.F.: Management and coordination responsibility for the research activity and execution Conceptualization, EES simulation, methodology, Writing—Original draft preparation, Manuscript preparation and data analysis, visualization. F.A.A.: Conceptualization, project administration, funding acquisition, Writing and manuscript editing, S.A.: Conceptualization, Writing and manuscript editing. M.A.A.: Conceptualization, Writing and manuscript editing. H.A.R.: Management and coordination responsibility for the research activity planning, Conceptualization, Data collection, visualization. All authors have read and agreed to the published version of the manuscript.

Funding: This research was funded by Researchers Supporting Project number (RSP2022R515), King Saud University, Riyadh, Saudi Arabia.

Institutional Review Board Statement: Not applicable.

Informed Consent Statement: Not applicable.

Data Availability Statement: Not applicable.

Acknowledgments: The authors extend their appreciation to the Researchers Supporting Project number (RSP2022R515), King Saud University, Riyadh, Saudi Arabia for funding this research work.

Conflicts of Interest: The authors declare no conflict of interest.

Nomenclature

A	Area, m ²
C _p	Specific heat, kJ/kg K
F ₁ , F ₂	Combined potential, –
h _{fg}	Water latent heat of evaporation, kJ/kg
h	Specific enthalpy, kJ/kg
I _T	Total solar intensity, W/m ²
m [•]	Mass flow rate, kg/s
Q [•]	Heat transfer rate, kW
t	Temperature, °C
W	Humidity ratio, g _v /kg _a
W [•]	Power, kW
Greek symbols	
η	Efficiency
η _{F1} , η _{F2}	Efficiency of the desiccant wheel
ε	Effectiveness
Δτ	Time, hours
Subscript	
a	Air/dry air/actual
atm	Atmosphere
avg	Average
BS	Basic system
cond	Condenser
Evap	Evaporator
g	Generator
hum	Humidifier
HE	Heat exchanger
i = 1, 2, 3	Index referring to various positions of the desiccant system
imp	Improvement
in	Input
ind	independent
ma	Moist air
v	Water vapour
reg	Regeneration
R,a	Return air
P,a	Process air
P	Pump
t	Turbine
w	Seawater
1, 2, 3, ...	State points

Abbreviations

BS	Basic system
COP	Coefficient of performance
DCS	Desiccant cooling system
GOR	Gain output ratio
HDH	Humidification dehumidification
ICE	Internal combustion engine
IS-I	Improved system-I
IS-II	Improved system-II
KSA	Kingdom of Saudi Arabia

LBSE	lithium bromide–water simple effect
MR	Mass flow rate ratio
MED	Multi-effect desalination
ORC	Organic Rankine cycle
RO	Reverse osmosis
SOFC	Solid oxide fuel cell
STG	Specific total gained energy, kWh/m ²
STGP	Specific total gained energy equivalent price, USD/ m ²
TGOR	Total gained output ratio

References

- Mehrpooya, M.; Sharifzadeh, M.M.M.; Rosen, M.A. Energy and exergy analyses of a novel power cycle using the cold of LNG (liquefied natural gas) and low-temperature solar energy. *Energy* **2016**, *95*, 324–345. [[CrossRef](#)]
- Karellas, S.; Braimakis, K. Energy–exergy analysis and economic investigation of a cogeneration and trigeneration ORC–VCC hybrid system utilizing biomass fuel and solar power. *Energy Convers. Manag.* **2016**, *107*, 103–113. [[CrossRef](#)]
- Wang, J.; Wu, J.; Zheng, C. Analysis of tri-generation system in combined cooling and heating mode. *Energy Build.* **2014**, *72*, 353–360. [[CrossRef](#)]
- Ahmadi, P.; Dincer, I.; Rosen, M.A. Performance assessment and optimization of a novel integrated multigeneration system for residential buildings. *Energy Build.* **2013**, *67*, 568–578. [[CrossRef](#)]
- Liu, H.; Zhou, Q.; Zhao, H.; Wang, P. Experiments and thermal modeling on hybrid energy supply system of gas engine heat pumps and organic Rankine cycle. *Energy Build.* **2015**, *87*, 226–232. [[CrossRef](#)]
- Jradi, M.; Riffat, S. Tri-generation systems: Energy policies, prime movers, cooling technologies, configurations and operation strategies. *Renew. Sustain. Energy Rev.* **2014**, *32*, 396–415. [[CrossRef](#)]
- Zhang, X.; Li, H.; Liu, L.; Zeng, R.; Zhang, G. Analysis of a feasible trigeneration system taking solar energy and biomass as co-feeds. *Energy Convers. Manag.* **2016**, *122*, 74–84. [[CrossRef](#)]
- Maraver, D.; Uche, J.; Royo, J. Assessment of high temperature organic Rankine cycle engine for polygeneration with MED desalination: A preliminary approach. *Energy Convers. Manag.* **2012**, *53*, 108–117. [[CrossRef](#)]
- Gholizadeh, T.; Vajdi, M.; Rostamzadeh, H. Exergoeconomic optimization of a new trigeneration system driven by biogas for power, cooling, and freshwater production. *Energy Convers. Manag.* **2020**, *205*, 112417. [[CrossRef](#)]
- Baghernejad, A.; Yaghoubi, M.; Jafarpur, K. Exergoeconomic comparison of three novel trigeneration systems using SOFC, biomass and solar energies. *Appl. Therm. Eng.* **2016**, *104*, 534–555. [[CrossRef](#)]
- Zare, V. A comparative thermodynamic analysis of two tri-generation systems utilizing low-grade geothermal energy. *Energy Convers. Manag.* **2016**, *118*, 264–274. [[CrossRef](#)]
- Azhar, M.S.; Rizvi, G.; Dincer, I. Integration of renewable energy based multigeneration system with desalination. *Desalination* **2016**, *404*, 72–78. [[CrossRef](#)]
- Gholizadeh, T.; Vajdi, M.; Rostamzadeh, H. A new trigeneration system for power, cooling, and freshwater production driven by a flash-binary geothermal heat source. *Renew. Energy* **2020**, *148*, 31–43. [[CrossRef](#)]
- Li, J.; Zoghi, M.; Zhao, L. Thermo-economic assessment and optimization of a geothermal-driven tri-generation system for power, cooling, and hydrogen production. *Energy* **2022**, *244*, 123151. [[CrossRef](#)]
- Hands, S.; Sethuvenkatraman, S.; Peristy, M.; Rowe, D.; White, S. Performance analysis & energy benefits of a desiccant based solar assisted trigeneration system in a building. *Renew. Energy* **2016**, *85*, 865–879.
- Abdelhay, A.; Fath, H.S.; Nada, S.A. Solar driven polygeneration system for power, desalination and cooling. *Energy* **2020**, *198*, 117341. [[CrossRef](#)]
- Dabwan, Y.N.D.; Pei, G.; Gao, G.; Feng, J.; Li, J. A novel integrated solar tri-generation system for cooling, freshwater and electricity production purpose: Energy, economic and environmental performance analysis. *Sol. Energy* **2020**, *198*, 139–150. [[CrossRef](#)]
- Yao, E.; Wang, H.; Wang, L.; Xi, G.; Maréchal, F. Multi-objective optimization and exergoeconomic analysis of a combined cooling, heating and power based compressed air energy storage system. *Energy Convers. Manag.* **2017**, *138*, 199–209. [[CrossRef](#)]
- Bellos, E.; Tzivanidis, C. Multi-objective optimization of a solar driven trigeneration system. *Energy* **2018**, *149*, 47–62. [[CrossRef](#)]
- Fouda, A.; Elattar, H.; Rubaiee, S.; Bin Mahfouz, A.S.; Alharbi, A.M. Thermodynamic and Performance Assessment of an Innovative Solar-Assisted Tri-Generation System for Water Desalination, Air-Conditioning, and Power Generation. *Eng. Technol. Appl. Sci. Res.* **2022**, *12*, 9316–9328. [[CrossRef](#)]
- Dincer, I.; Demir, M.E. Comprehensive Energy Systems, Chapter 4.8. In *Steam and Organic Rankine Cycles*; Elsevier: Amsterdam, The Netherlands, 2018; pp. 4–5.
- Elattar, H.; Fouda, A.; Nada, S. Performance investigation of a novel solar hybrid air conditioning and humidification–dehumidification water desalination system. *Desalination* **2016**, *382*, 28–42. [[CrossRef](#)]
- Eldean, M.A.S.; Soliman, A.M. Study of Using Solar Thermal Power for the Margarine Melting Heat Process. *J. Sol. Energy Eng.* **2015**, *137*, 021004–2100413.

24. Walraven, D.; Laenen, B.; D'Haeseleer, W. Comparison of thermodynamic cycles for power production from low-temperature geothermal heat sources. *Energy Convers. Manag.* **2013**, *66*, 220–233. [[CrossRef](#)]
25. Panaras, G.; Mathioulakis, E.; Belessiotis, V.; Kyriakis, N. Theoretical and experimental investigation of the performance of a desiccant air-conditioning system. *Renew. Energy* **2010**, *35*, 1368–1375. [[CrossRef](#)]
26. Wang, N.; Wang, D.; Dong, J.; Wang, H.; Wang, R.; Shao, L.; Zhu, Y. Performance assessment of PCM-based solar energy assisted desiccant air conditioning system combined with a humidification-dehumidification desalination unit. *Desalination* **2020**, *496*, 114705. [[CrossRef](#)]
27. Ayompe, L.; Duffy, A. Thermal performance analysis of a solar water heating system with heat pipe evacuated tube collector using data from a field trial. *Sol. Energy* **2013**, *90*, 17–28. [[CrossRef](#)]
28. Zhang, T.; Ma, J.; Zhou, Y.; Wang, Y.; Chen, Q.; Li, X.; Liu, L. Thermo-economic analysis and optimization of ICE-ORC systems based on a splitter regulation. *Energy* **2021**, *226*, 120271. [[CrossRef](#)]
29. Zubair, S.M.; Antar, M.A.; Elmutasim, S.; Lawal, D.U. Performance evaluation of humidification-dehumidification (HDH) desalination systems with and without heat recovery options: An experimental and theoretical investigation. *Desalination* **2018**, *436*, 161–175. [[CrossRef](#)]
30. Galloni, E.; Fontana, G.; Staccone, S. Design and experimental analysis of a mini ORC (organic Rankine cycle) power plant based on R245fa working fluid. *Energy* **2015**, *90*, 768–775. [[CrossRef](#)]
31. Tehrani, S.S.M.; Saffar-Avval, M.; Mansoori, Z.; Kalhori, S.B.; Abbassi, A.; Dabir, B.; Sharif, M. Development of a CHP/DH system for the new town of Parand: An opportunity to mitigate global warming in Middle East. *Appl. Therm. Eng.* **2013**, *59*, 298–308. [[CrossRef](#)]
32. Choi, J.H.; Ahn, J.H.; Kim, T.S. Performance of a triple power generation cycle combining gas/steam turbine combined cycle and solid oxide fuel cell and the influence of carbon capture. *Appl. Therm. Eng.* **2014**, *71*, 301–309.
33. Fouda, A.; Nada, S.A.; Elattar, H.F. An integrated A/C and HDH water desalination system assisted by solar energy: Transient analysis and economical study. *Appl. Therm. Eng.* **2016**, *108*, 1320–1335. [[CrossRef](#)]
34. Puig-Arnavat, M.; Bruno, J.C.; Coronas, A. Modeling of trigeneration configurations based on biomass gasification and comparison of performance. *Appl. Energy* **2014**, *114*, 845–856. [[CrossRef](#)]
35. Fahad, A. Al-Sulaiman, Ibrahim Dincer, Feridun Hamdullahpur, Energy analysis of a trigeneration plant based on solid oxide fuel cell and organic Rankine cycle. *Int. J. Hydrog. Energy* **2010**, *35*, 5104–5113.
36. Huang, Y.; Wang, Y.D.; Rezvani, S.; McIlveen-Wright, D.R.; Anderson, M.; Mondol, J.; Zacharopoulos, A.; Hewitt, N.J. A techno-economic assessment of biomass fuelled trigeneration system integrated with organic Rankine cycle. *Appl. Therm. Eng.* **2013**, *53*, 325–331. [[CrossRef](#)]
37. Nada, S.A.; Fouda, A.; Mahmoud, M.A.; Elattar, H.F. Experimental investigation of air-conditioning and HDH desalination hybrid system using new packing pad humidifier and strips-finned helical coil. *Appl. Therm. Eng.* **2021**, *185*, 116433. [[CrossRef](#)]